Front. Earth Sci. 2019, 13(2): 277–289
https://doi.org/10.1007/s11707-019-0750-3

RESEARCH ARTICLE

Bias characterization of ATMS low-level channels under clear-sky and cloudy conditions

Qi LI[1], Xiaolei ZOU (✉)[2]

1 Joint Center of Data Assimilation for Research and Application, College of Atmospheric Science, Nanjing University of Information Science and Technology (NUIST), Nanjing 210044, China
2 Earth System Science Interdisciplinary Center (ESSIC), University of Maryland, College Park, MD 20740-3823, USA

Abstract The Advanced Technology Microwave Sounder (ATMS) onboard the Suomi National Polar-Orbiting Partnership satellite is a cross-track scanning instrument containing 22 sounding channels in total. In this study, the bias characteristics of channels 1–6, which could have significant cloud contamination in heavy precipitation, are first analyzed based on the differences between ATMS observations (O) and model simulations (B) under clear-sky conditions over oceans. Latitudinal dependencies of the biases of window channels 1–3 are greater than those of channels 4–6. Biases of all nadir-only observations examined in different latitudinal bands [$\mu_1(\varphi)$] are positive and no more than 7.0 K. Biases at higher latitudes are larger. Channels 1–5 have a generally symmetric scan bias pattern [$\mu_2(\alpha)$]. The global distributions of brightness temperature differences after subtracting the biases, i.e., O-B-$\mu_1(\varphi)$-$\mu_2(\alpha)$, for channels 3–6 spatially match the liquid water path distributions. Excluding ice-affected observations, channel 3–6 O-B differences systematically increase as the liquid water path increases under cloudy conditions. Further investigation is needed to apply these findings for ATMS data assimilation under both clear-sky and cloudy conditions.

Keywords ATMS, O-B, clear-sky bias characteristics, impact of clouds on biases

1 Introduction

On 28 October 2011, the Suomi National Polar-orbiting Partnership (S-NPP) satellite was successfully launched into a sun-synchronous orbit at a nominal altitude of 824 km and an inclination angle of ~98.7° to the equator. The equator crossing time of the S-NPP satellite is 1330 local time at its ascending node. The Advanced Technology Microwave Sounder (ATMS) onboard the S-NPP satellite contains 22 detecting channels in total, and their frequencies range from 23 to 183 GHz. The instrument has inherited most of the sounding channels from its predecessors: the Advanced Microwave Sounding Unit A (AMSU-A) and the Microwave Humidity Sounder (MHS) onboard National Oceanic and Atmospheric Administration (NOAA) and Europe's Meteorological Operational (MetOp) satellites. Zou et al. (2013) assessed the impact of ATMS data assimilation on hurricane track and intensity forecasts. Bormann et al. (2013) evaluated the impact of assimilating ATMS observed radiances on global medium-range forecasts. A modified hurricane warm-core retrieval algorithm was developed by Tian and Zou (2016) to obtain the warm-core structures of hurricanes from both ATMS and AMSU-A brightness temperature observations. ATMS data is also used operationally at the UK Met Office. Doherty et al. (2015) made an initial assessment of the data within this operational system.

ATMS bias characterization has been done for the upper tropospheric temperature-sounding channels 7–15 (Zou et al., 2014). This study examines the ATMS bias characteristics in both clear and cloudy skies for middle and lower tropospheric window channels 1–6. Such a study is important for ATMS data assimilation (Dee, 2005; Auligné et al., 2007). The differences in brightness temperature between observations and model simulations is a widely used way of examining instrument biases. Wang and Zou (2012) assessed the quality of brightness temperature measurements of upper-level sounding channels from the FengYun-3B microwave temperature sounder (MWTS) by comparing them with numerical weather prediction (NWP) model simulations. The central frequencies of the three MWTS upper-level sounding

Received November 18, 2018; accepted March 18, 2019

E-mail: xzou1@umd.edu

channels shifted after the FengYun-3B satellite launched into orbit. Wang et al. (2012) showed that this could induce a strong temperature dependence of MWTS biases. Weng et al. (2012) described the characteristics of the ATMS instrument and showed some preliminary results on the bias characteristics of upper-level sounding channels 5–15 under clear-sky conditions over oceans using the National Centers for Environmental Prediction (NCEP) global forecast system (GFS) 6-h forecast fields of the atmospheric states during 20–27 December 2011. The NCEP GFS 6-h forecast fields have a horizontal resolution 0.3125°×0.3125° and 64 vertical levels from the earth's surface to ~0.01 hPa. Zou et al. (2014) proposed to use Global Positioning System radio occultation observations to quantify the biases at the ATMS upper-level sounding channels.

In most published studies, a large number of observations from surface-sensitive channels over land are eliminated by quality control due to the effects of clouds and surface emissivity. With a better estimation of the surface emissivity and surface skin temperature, Karbou et al. (2006, 2010a, b) showed that the assimilation of the surface-sensitive channels of the AMSU has a significant positive impact on NWP in the Southern Hemisphere, especially in West Africa. An investigation of the impacts of clouds and surface emissivity on the surface-sensitive channels of the ATMS has yet to be done.

The paper is organized as follows. Section 2 briefly describes the ATMS channel characteristics and model simulations. Section 3 presents numerical results showing the ATMS bias characteristics under clear-sky conditions. These include latitudinal-dependent biases [$\mu(\varphi)$] and scan-angle dependent biases [$\mu(\alpha)$] for channels 1–6. Section 4 discusses the impacts of liquid and ice clouds on ATMS channel 3–6 observations. Section 5 summarizes the study and draws conclusions.

2 ATMS channel characteristics and model simulations

2.1 ATMS channel characteristics

The ATMS is a total-power cross-track scanning radiometer. Each scan line contains 96 fields of view (FOVs). The ATMS scanning angle is within ±52.7°, which is wider than that of the AMSU-A (±48.3°), and the orbital gap between adjacent orbits is very small even in the tropics. The central frequencies of ATMS channels 4–15, which are used to detect global atmospheric temperatures from the surface to about 1 hPa (~45 km), are located near the oxygen absorption band (50–60 GHz). The central frequencies of channels 18–22 are located near the 183-GHz water vapor absorption line and are used to detect atmospheric humidity from the ground to 200 hPa (~10 km; Weng et al., 2012).

Figure 1 shows the vertical distribution of the weighting functions of the 22 ATMS channels calculated by inputting the U.S. standard profile to the Community Radiative Transfer Model (CRTM) developed by the U.S. Joint Center for Satellite Data Assimilation (Han et al., 2007; Weng, 2007). Table 1 lists the center frequencies, beam widths, and altitudes of these weighting functions. The bias characteristics of the first six low-frequency channels of the ATMS are investigated. Channels 1 and 2 are window channels that are highly sensitive to the surface and clouds and less sensitive to atmospheric radiation. The peak heights of the weighting functions for channels 4–6 are 950 hPa, 850 hPa and 700 hPa, respectively. The horizontal resolution of a microwave sounder is defined by the FOV sizes, which depend on the S-NPP satellite height, scanning angles, and beam widths. The beam width for ATMS window channels 1–2 is 5.2°, corresponding to a 75-km diameter, nearly circular footprint on the ground at nadir. Channels 3–6 beam widths are 2.2°, corresponding to a 32-km diameter, nearly circular FOVs at nadir.

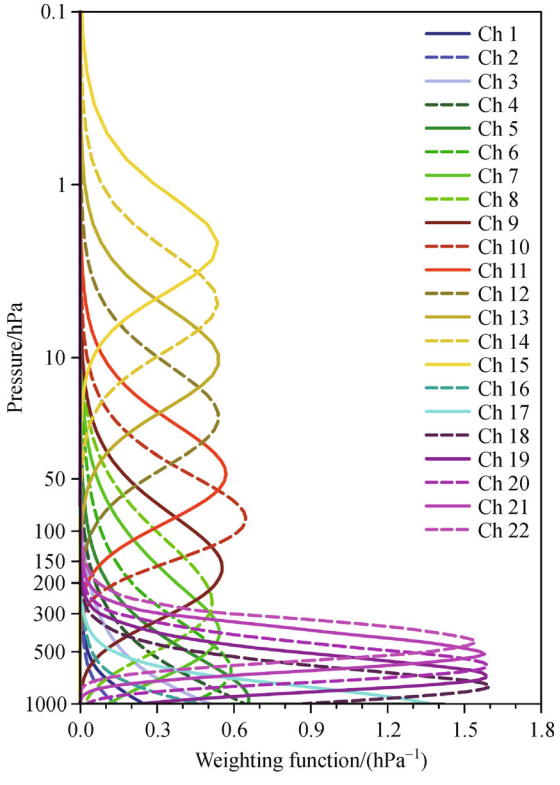

Fig. 1 Weighting functions of the 22 ATMS channels.

2.2 Model simulations

The forward radiative transfer model used in this study is the CRTM. This model can be used to simulate a variety of radiation instruments covering the microwave, infrared, and visible bands, such as the AMSU-A, the cross-track infrared sounder, and the ATMS (Han et al., 2007; Weng,

Table 1 Instrument characteristics of the ATMS

Channel	Center frequency /GHz	Beam width /deg	Weighting function peak /hPa
1	23.8	5.2	Window
2	31.4	5.2	Window
3	50.3	2.2	Window
4	51.76	2.2	950
5	52.8	2.2	850
6	53.596±0.115	2.2	700
7	54.40	2.2	400
8	54.94	2.2	250
9	55.50	2.2	200
10	57.29	2.2	100
11	57.29±0.217	2.2	50
12	57.29±0.322±0.048	2.2	25
13	57.29±0.322±0.022	2.2	10
14	57.29±0.322±0.010	2.2	5
15	57.29±0.322±0.0045	2.2	2
16	88.2	2.2	Window
17	165.5	1.1	Window
18	183.31±7	1.1	800
19	183.31±4.5	1.1	700
20	183.31±3	1.1	500
21	183.31±1.8	1.1	400
22	183.31±1.0	1.1	300

2007). The initial CRTM version was released in 2004 and was subsequently improved. This study uses version 2.2.3 of the model.

Simulated brightness temperatures of the ATMS are obtained using the background field as the input field of the CRTM. This study uses reanalysis data at a horizontal resolution of 0.75°×0.75° from the European Center for Medium-Range Weather Forecasts (ECMWF) at 0000, 0600, 1200, and 1800 coordinated universal time (UTC). There are 37 levels in the vertical direction, and the top-level pressure is approximately 1 hPa. Input background variables include the 10-m zonal wind component, the 2-m dew-point temperature, the surface skin temperature, the 2-m temperature, the surface pressure, the 10-m meridional wind component, as well as atmospheric pressure, water vapor mixing ratio, and atmospheric temperature fields. Also inputted to the CRTM are instrument parameters such as scan angle and zenith angle. The ECMWF analyses are linearly interpolated in the temporal and horizontal dimensions onto the ATMS-observed pixel locations and times.

Data from 1–30 January, 1–30 April, 1–30 July, and 1–30 October 2015 are used to calculate the differences between ATMS-observed brightness temperatures and model-simulated brightness temperatures. At present, the model simulation accuracy is higher under clear-sky conditions than under cloudy conditions (Zou et al., 2016). Only data over oceans are used to minimize the influence of uncertainties in the land surface emissivity and clouds on the bias estimation. ATMS pixels near the coast may be partially located over both land and sea. Therefore, pixels within 30 km of coastlines are excluded. Most of the ocean area at high latitudes is covered by sea ice, so only data within the latitudes of 55°S and 55°N are considered.

3 ATMS bias characteristics

An important application of ATMS-observed radiances is to improve global medium-range forecasts through data assimilation. Minimum variance estimation or maximum likelihood estimation forms the basis of all data assimilation theories. However, the underlying assumption is that both observations (O) and model simulations (B) are unbiased. Any bias related to the instrument and model simulations needs to be quantified then removed in satellite data assimilation. It is, therefore, necessary to estimate the biases of the instrument and the model before using the data.

Biases in satellite observations arise from the sensitivity of the instrument calibration, the presence of clouds, and the response characteristics of sensors. Regarding model simulations, both the radiative transfer model and the background field could contain biases. The observation bias and the model bias can be expressed as

$$(\mathrm{O}-\mu^{\mathrm{o}})-(\mathrm{B}-\mu^{\mathrm{b}})=\mathrm{O}-\mathrm{B}-(\mu^{\mathrm{o}}+\mu^{\mathrm{b}}), \quad (1)$$

where μ^{o} and μ^{b} are the observation and model biases, respectively. Eq. (1) shows that O-B statistics can estimate the sum biases of instrument observations and model simulations. Four months of ATMS observations under clear-sky conditions are first used to characterize the performance of the ATMS window and low-level sounding channels 1–6. Cloud-affected ATMS FOVs are then used to examine cloud impacts on ATMS observations.

3.1 Cloud liquid water path (LWP) retrievals from ATMS window channels

The LWP over oceans can be calculated using the following formula:

$$\mathrm{LWP}=\alpha_0\mu[\ln(T_s-T_b^{ch2})-\alpha_1\ln(T_s-T_b^{ch1})-\alpha_2], \quad (2)$$

where

$$\alpha_0=-0.5k_v^{ch1}/(k_v^{ch1}k_l^{ch2}-k_v^{ch2}k_l^{ch1}), \quad (3)$$

$$\alpha_1=k_v^{ch2}/k_v^{ch1}, \quad (4)$$

and

$$\alpha_2 = -2.0(\tau_0^{ch2} - \alpha_1 \tau_0^{ch1})/\mu + (1.0 - \alpha_1)\ln(T_s) + \ln(1.0 - \varepsilon^{ch2}) - \alpha_1 \ln(1.0 - \varepsilon^{ch1}). \quad (5)$$

Brightness temperatures of channel 1 and channel 2 are represented by T_b^{ch1} and T_b^{ch2}, respectively. The variable T_s is the sea surface temperature, k_l is the cloud liquid water mass absorption coefficient, k_v is the water vapor mass absorption coefficient, ε is the surface emissivity, τ_0 is the optical thickness, and θ is the satellite zenith angle, $\mu = \cos\theta$. The LWP threshold usually used to determine whether or not an ATMS FOV is affected by a cloud is 0.01 kg·m^{-2}. ATMS pixels with LWPs less than 0.01 kg·m^{-2} are selected here for obtaining reliable clear-sky bias estimates.

Figures 2(a) and 2(b) show the global distributions of observed brightness temperatures at channels 1 and 2 for ATMS ascending nodes on 17 July 2015. There are clear differences in brightness temperature between oceans and land for ATMS window channels 1–2, which are sensitive to the earth's surface. There is also almost no gap between the adjacent orbits of the ATMS, which is especially important for the observation of tropical cyclones at low latitudes. Figure 2(c) shows LWP retrievals derived from the ATMS window channels at 23.8 and 31.4 GHz. The minimum value is 0, and the maximum value is 2 kg·m^{-2}.

Figure 3(a) shows the spatial distribution of the number of ATMS clear-sky pixels within 5°×5° grid boxes over oceans within the four-month sampling period. There are more than 40,000 clear-sky pixels in each grid box in the middle and low latitudes. Figure 3(b) shows the number of data samples with respect to scan position and latitude. A

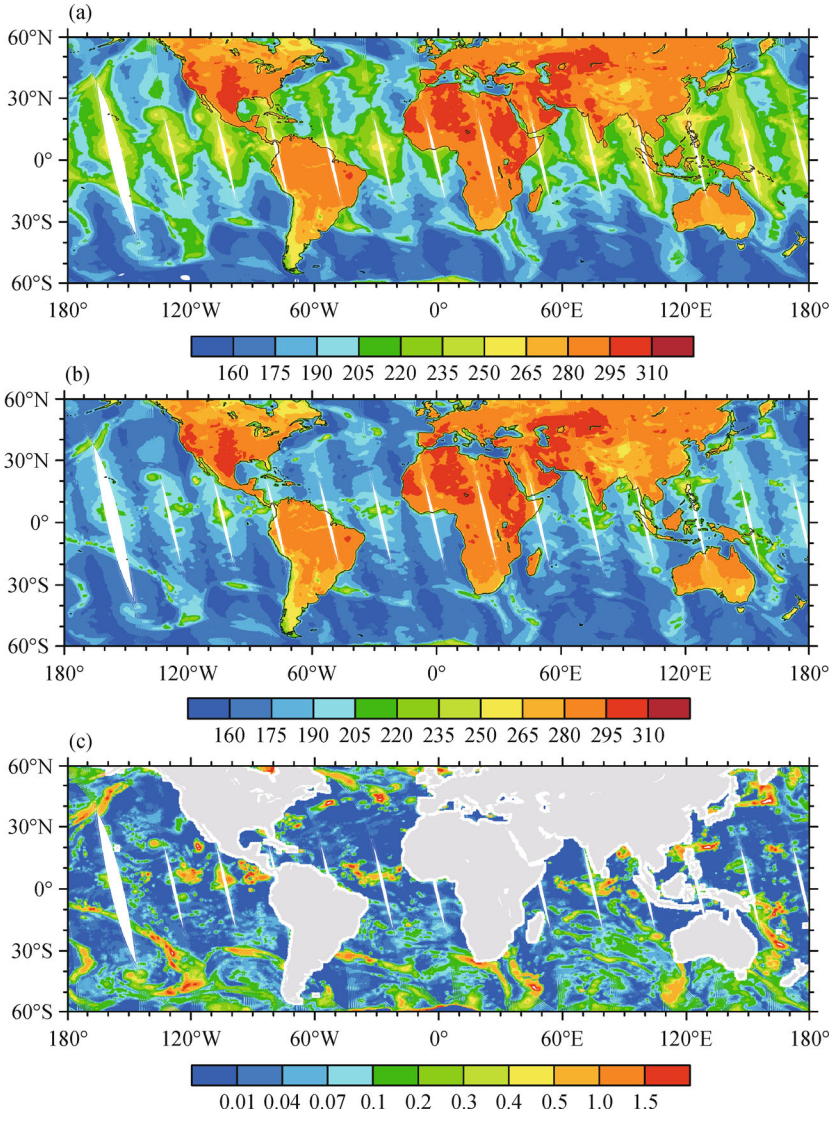

Fig. 2 Global distributions of (a) channel 1 and (b) channel 2 brightness temperatures (unit: K), as well as (c) LWP retrievals over oceans (unit: kg·m^{-2}) for ATMS ascending nodes on 17 July 2015.

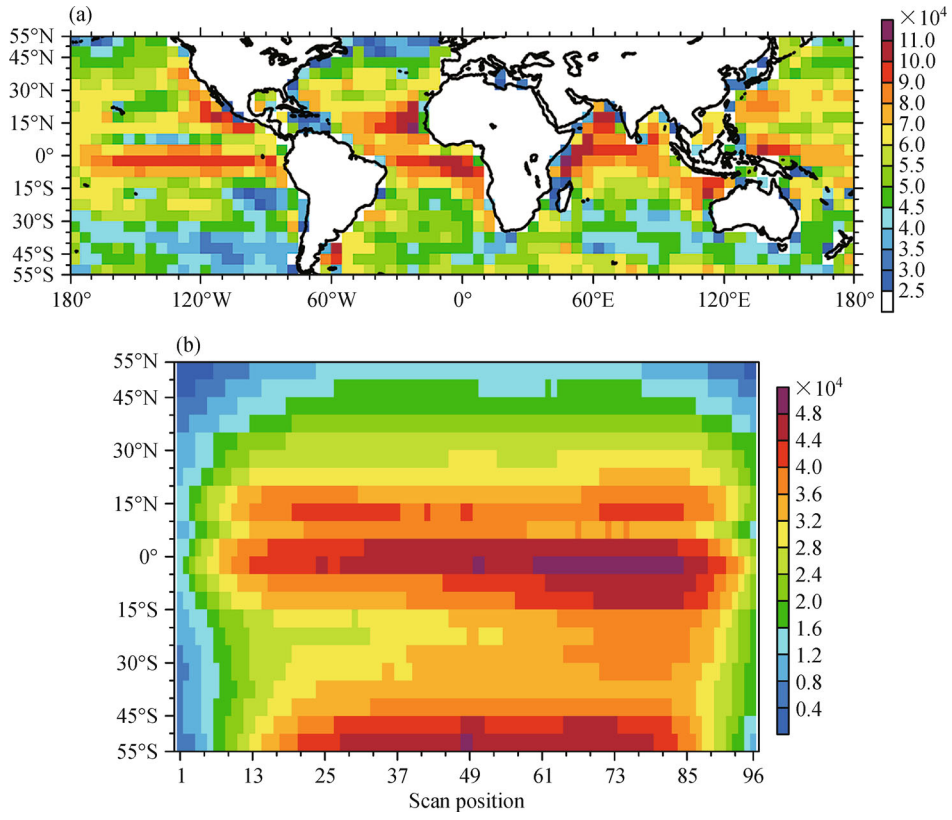

Fig. 3 (a) Spatial distributions of ATMS clear-sky data counts within 5°×5° grid boxes over oceans and (b) the number of data samples with respect to scan position and latitude. Data are from 1–30 January, 1–30 April, 1–30 July, and 1–30 October 2015.

sufficient amount of ATMS data can guarantee the accuracy of the ATMS bias estimates.

3.2 Latitudinal and scan-angle dependencies of biases

Figure 4 shows the latitudinal distributions of the O-B biases and standard deviations for ATMS channels 1–6 obtained within 5° latitudinal bands. Since observations at nadir are the most accurate, all data within 55°S and 55°N under clear-sky nadir-only conditions over oceans are used. The biases of window channels 1–3 are greater than those of channels 4–6. Overall, biases decrease in magnitude with detection height. Channel 1 has large positive biases in equatorial and low-latitude regions, which decrease gradually as the latitude increases. There is an increasing trend at high latitudes. Channel 2–3 positive biases are smaller in the low to mid-latitudes, gradually increasing as latitude increases. Channels 5–6 have mainly positive biases of ~0.5 K. The increase in biases for channels 1–6 near 55°S may be related to the scattering effect of sea ice. The standard deviations of all channels fluctuate at different latitudes and decrease with detection height, suggesting that the data becomes more stable as the detecting altitude increases.

For a cross-track scanning radiometer, the optical path length varies with the scanning angle, which is the main cause of the so-called limb effect. A fast RTM can model this limb effect. The side-lobe effect and the effect of atmospheric inhomogeneity introduced by spacecraft radiation on satellite observations increase as the scan angle increases (Zou et al., 2013). In NWP and data assimilation applications, it is necessary to quantify and remove all scan-angle biases. Figure 5 shows the brightness temperature biases for channels 1–6 as functions of scan position. To better show the scan-angle biases, the nadir bias calculated from the averaged brightness temperatures at FOVs 48 and 49 is subtracted from biases at each scan position. The bias distributions for channels 1–5 are generally symmetric, but that for channel 6 is not. The root cause of the channel 6 asymmetric bias pattern needs further study. The biases near the nadir are negligible for all channels examined. The channel 1–2 biases are positive and reach their maxima at larger scan-angle positions. The channel 3–6 biases are negative and reach their minima at larger scan-angle positions.

Biases vary with time on both diurnal and seasonal scales (Auligné et al., 2007). A time-varying bias correction scheme is used here, accounting for the regression cycle of the scan position. Figure 6(a) shows the nadir positions of the ATMS from 1–16 July 2015. The nadir position on the seventeenth day coincides with that on the first day, which indicates that the nadir drift cycle of

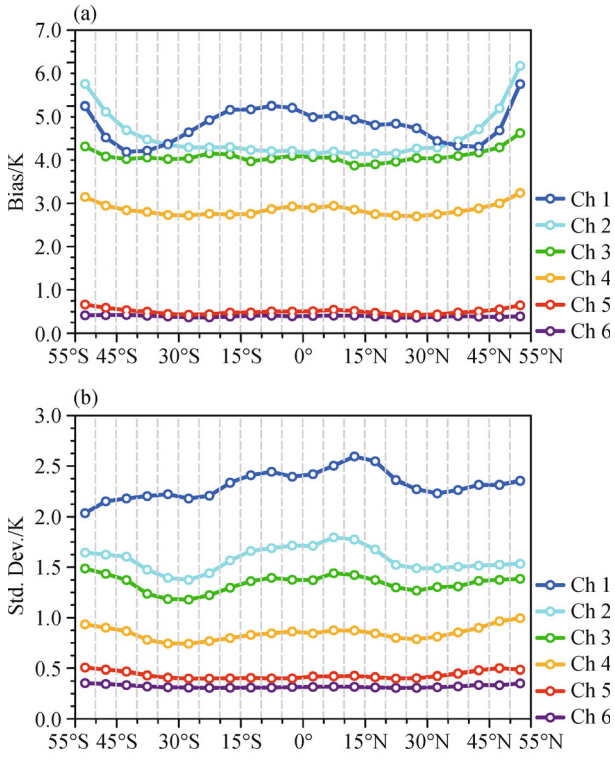

Fig. 4 Latitudinal dependencies of (a) O-B biases and (b) standard deviations for ATMS channels 1–6 obtained within 5° latitudinal bands from 55°S and 55°N under clear-sky nadir-only conditions over oceans. Data are from 1–30 January, 1–30 April, 1–30 July, and 1–30 October 2015.

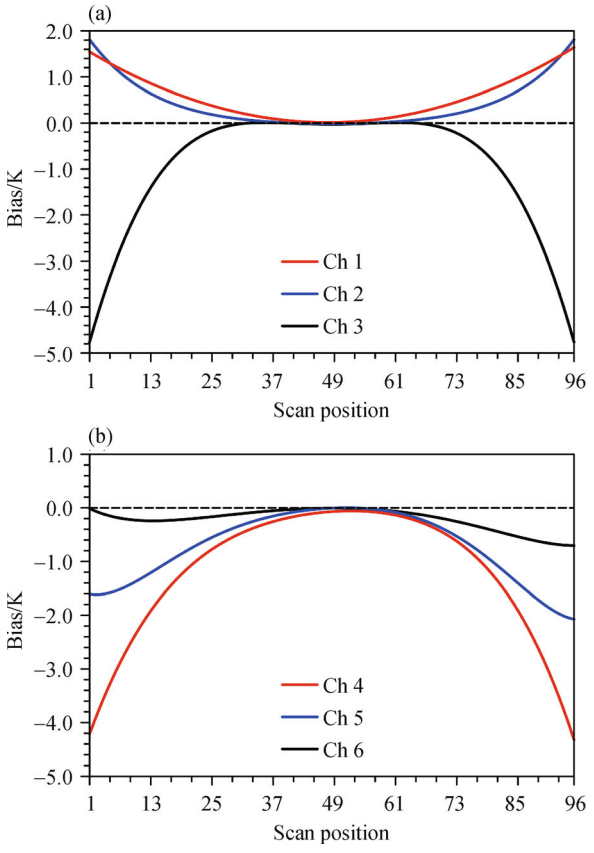

Fig. 5 Scan-dependent biases of ATMS channels (a) 1–3 and (b) 4–6 for all data within 55°S and 55°N under clear-sky conditions over oceans from 1–30 January, 1–30 April, 1–30 July, and 1–30 October 2015. The nadir bias has been subtracted.

the ATMS is 16 days (Fig. 6(b)). Data from 1–16 July 2015 are, therefore, used to calculate the bias for the bias correction on 17 July 2015. The latitudinal and scan-angle dependencies of biases obtained by using 16-day data are similar to those in Figs. 4 and 5, with only minor differences. These figures are omitted. Figure 7 shows the spatial distributions of corrected O-B [i.e., O-B-$\mu(\alpha)$-$\mu(\varphi)$] for ATMS channels 1–6 from ascending nodes within 55°S and 55°N over oceans on 17 July 2015. The latitudinal and scan-angle dependent biases [$\mu(\varphi)$, $\mu(\alpha)$] seen in Figs. 4 and 5 have been subtracted. The scan-dependent biases are barely seen in Fig. 7. Also, the spatial distributions of corrected O-B for each channel correspond well with LWP values (Fig. 2(c)). With the increase in detecting heights of channels 3–6, the influence of clouds becomes smaller, and the response of the corrected O-B to LWP becomes weaker for all channels examined.

4 The LWP dependence of O-B-$\mu(\alpha)$-$\mu(\varphi)$ for ATMS channels 3–6

The ATMS has temperature-sounding channels and humidity-sounding channels for use in LWP and IWP retrievals, respectively. To further study the LWP dependence of O-B biases, an algorithm developed by Zhao and Weng (2002) for the AMSU and recently modified by Xu and Zou (2018) is used for retrieving IWP from ATMS channel 16 and 17 measurements. Figure 8 shows the spatial distributions of IWP retrievals from the ATMS over oceans on 17 July 2015. Large IWP values generally correspond to large LWP values. The IWP here ranges from 0 to 2 kg·m^{-2}. As in the LWP case, 0.01 kg·m^{-2} is used as a threshold to determine whether cloud ice is present. If the IWP of an ATMS FOV is less than this threshold, the effect of cloud ice can be neglected.

Figure 9 shows the relationship between the corrected O-B bias for channels 3–6 and LWP on 17 July 2015. The biases of all channels examined gradually become more and more negative with the largest negative biases seen when coincident LWP and IWP values are at their largest. The presence of liquid water in clouds results in an additional emission in the frequency range of channels 3–6, which results in much higher observed brightness temperatures than simulated brightness temperatures assuming a "clear sky" in the absence of ice. The presence of ice in clouds will cause a scattering effect in the

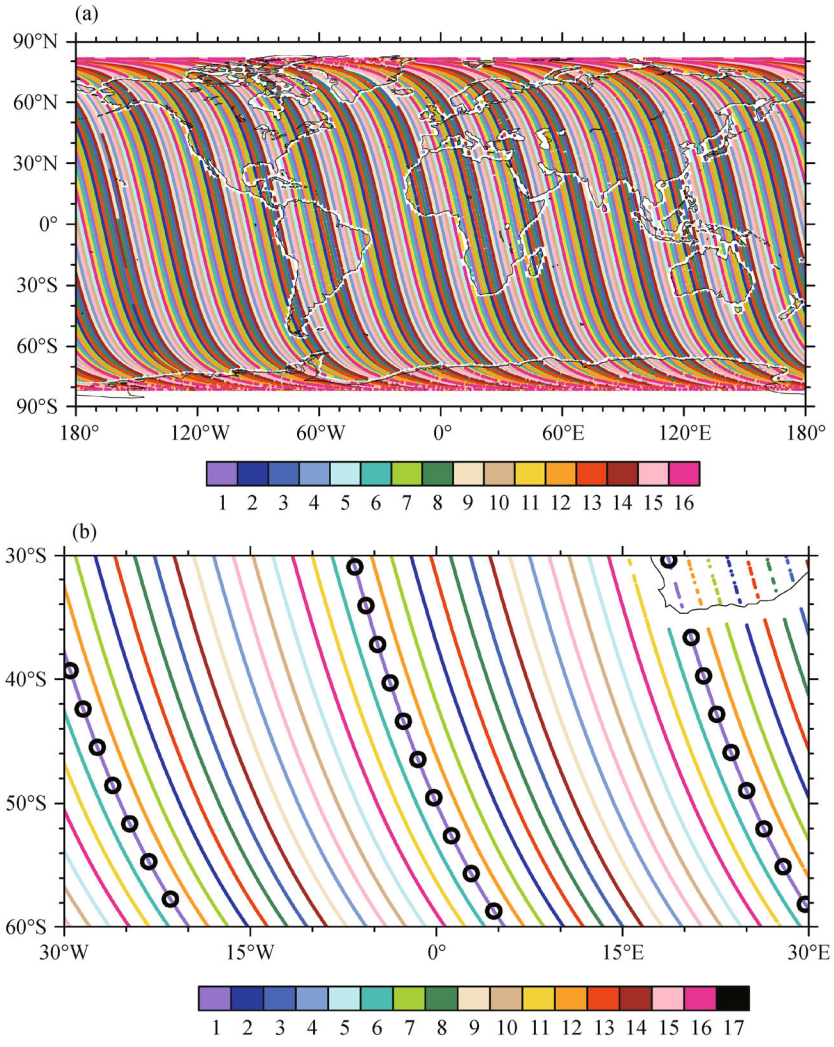

Fig. 6 (a) Nadir locations of ATMS ascending nodes from 1–16 July 2015. (b) Magnification of the area to the southwest of South Africa in Fig. 6(a) on 17 July 2015. The black circles show the nadir locations of the ATMS ascending nodes. Each color in the legend represents a date in the range of 1–16 July 2015.

frequency range of channels 3–6, which results in much lower observed brightness temperatures than simulated brightness temperatures assuming a "clear sky".

Figure 10 shows the LWP dependence of the corrected bias for ATMS channels 3–6 when data associated with IWP values greater than or equal to 0.01 $kg \cdot m^{-2}$ are excluded. Each channel shows different degrees of increase in corrected bias as LWP increases. This is because the cloud emissivity in the frequency range of channels 3–6 is higher than that of oceans. When skies are cloudy over oceans, the observed brightness temperatures are higher than when skies are clear over oceans. Figure 11 shows the mean biases and standard deviations in Fig. 10 before and after the bias correction as a function of LWP for ATMS channels 3–6. The mean biases of channels 3 and 4 after the bias correction are significantly reduced. From channel 3 to channel 6, the sensitivities of the corrected O-B to LWP in each channel decreases. Among them, channel 3 is the most sensitive. With the increase in the detection height of channels 4–6, the response gradually weakens. The LWP has little effect on the mean biases of channel 6. In terms of the standard deviation, as LWP increases, the dispersion of corrected O-B from channel 3 to channel 6 becomes increasingly larger. The higher the detection height, the smaller the influence of the earth's surface and clouds, and better overall stability is achieved.

Figure 12 is the same as Fig. 11 but for data on 17 July of the years 2012–2017. The latitudinal and scan dependencies of the biases are calculated using data from 1–16 July of each year. The trends in each channel change little over the different years. Small differences are seen when the LWP is greater than 0.5 $kg \cdot m^{-2}$. This may be related to the reduction in data counts in this LWP range.

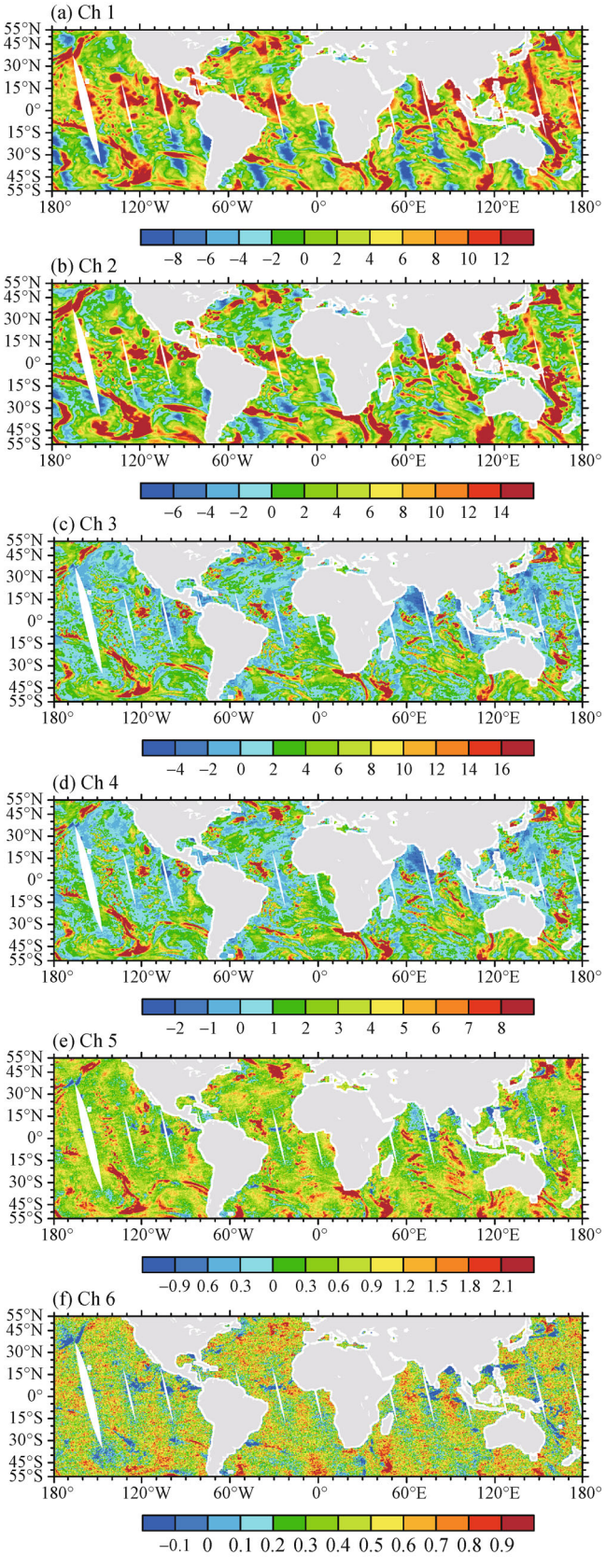

Fig. 7 Spatial distributions of the differences between observed brightness temperatures and model-simulated brightness temperatures (unit: K) without scan- and latitude-dependent biases for ATMS channels 1–6 (panels (a) to (f), respectively) from ascending nodes within 55°S and 55°N over oceans on 17 July 2015.

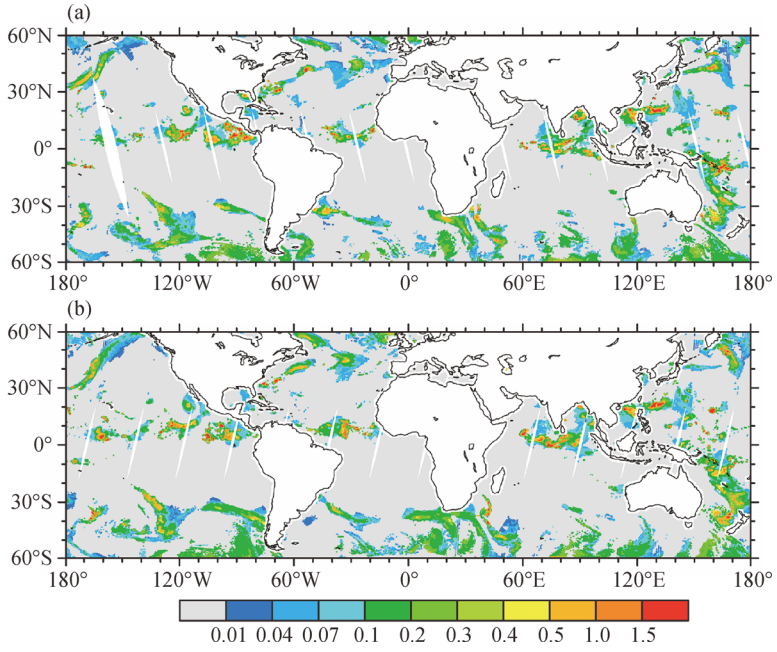

Fig. 8 Spatial distributions of IWP retrievals (unit: kg·m^{-2}) from the ATMS over oceans from (a) ascending and (b) descending nodes within 60°S and 60°N on 17 July 2015.

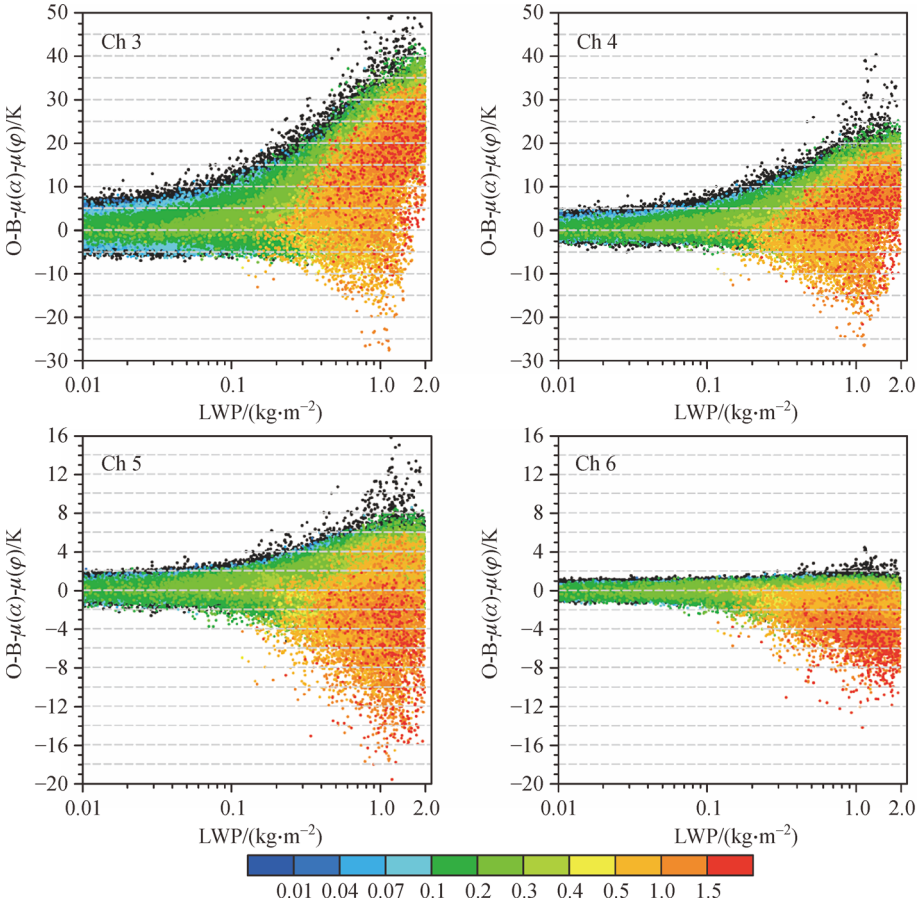

Fig. 9 IWP (coloured dots; unit: kg·m^{-2}) as a function of LWP and the corrected O-B bias for ATMS channels 3–6 within 55°S and 55°N under cloudy conditions over oceans on 17 July 2015. Black dots show data with IWP values less than 0.01 kg·m^{-2}.

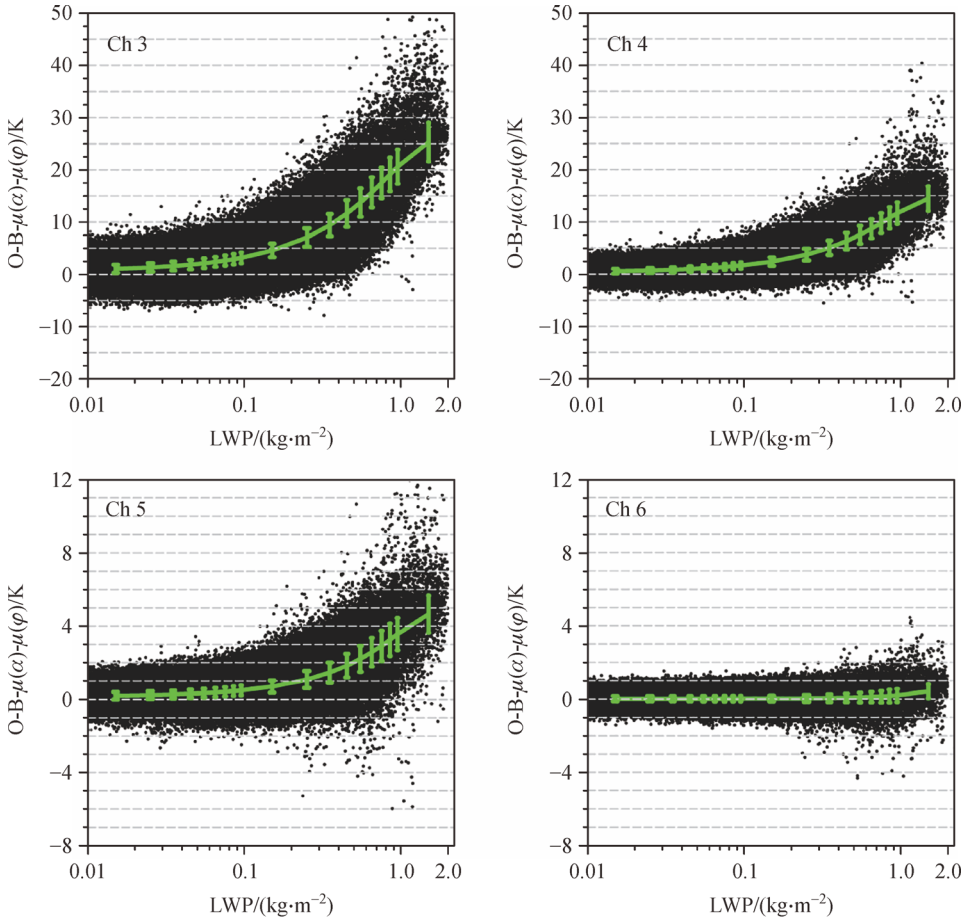

Fig. 10 Same as Fig. 9 except that data with IWP values greater than or equal to 0.01 kg·m^{-2} are excluded. Mean biases and standard deviations in each LWP bin are shown in green.

Using the dependence of corrected O-B on LWP, the biases under cloudy conditions can be corrected. Figure 13 shows the global distributions of O-B without scan-, latitude-, and LWP-dependent biases, i.e., O-B-$\mu(\alpha)$-$\mu(\varphi)$-μ(LWP), for ATMS channels 3–6 from ascending nodes within 55°S and 55°N over oceans on 17 July 2015. The LWP dependent biases [μ(LWP)] seen in Fig. 11 have been subtracted. Compared with Fig. 7, the bias is significantly reduced in cloudy areas. This suggests that after applying a proper bias correction, data associated with smaller LWPs can be used as clear-sky points for clear-sky assimilation. The impact of this on NWP will be evaluated in a follow-on study using an assimilation system.

5 Summary and conclusions

In this study, bias characteristics of the six low-level and lowest-frequency ATMS channels are estimated using the differences in brightness temperature between ATMS observations and CRTM simulations under clear-sky conditions over oceans. Excluded are mixed land/water pixels within 30 km of coastlines. This study employed ATMS data from four months in 2015 to ensure a sufficiently large data sample.

The biases have latitudinal and scan-angle dependencies for all channels examined. The biases of surface-sensitive channels 2–3 are positive with small biases in the low and mid-latitudes and large biases in the high latitudes. The channel-1 biases have the reverse pattern. Channels 5–6 have positive biases of ~0.5 K. The latitudinal dependence of the biases increases near 55°S for all channels examined, which may be related to the scattering effect of sea ice. As a cross-track sounder, the scan biases for all channels are mainly in the large scan positions reflecting the limb effect. Channels 1–5 show symmetric scan bias features but not channel 6. The scan biases of channels 1–2 are positive but negative for channels 3–6.

The spatial distribution of the bias-corrected O-B differences, i.e., O-B-$\mu(\alpha)$-$\mu(\varphi)$, in each channel corresponds well with the spatial distribution of LWP. An algorithm developed to retrieve IWP from ATMS channels

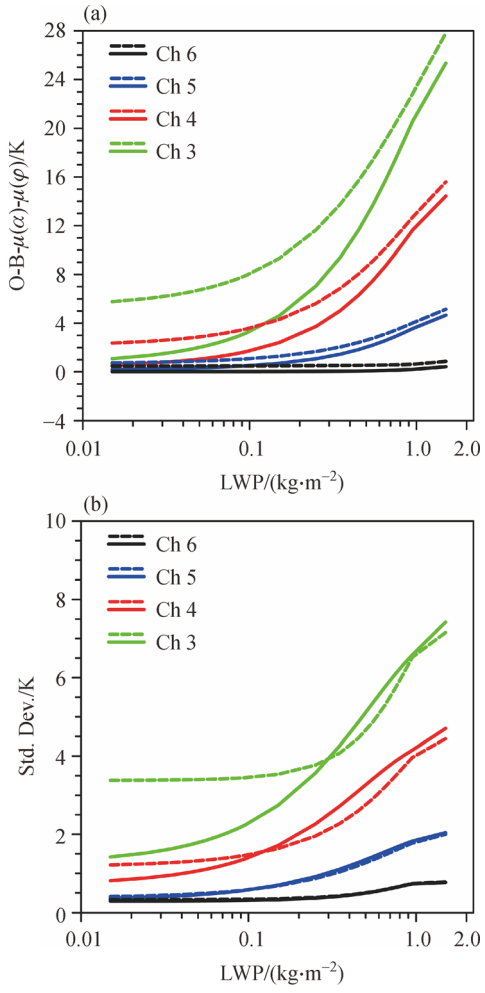

Fig. 11 (a) The mean biases and (b) standard deviations of O-B before (dashed curves) and after (solid curves) the bias correction with respect to LWP for ATMS channels 3–6. Data falling within 55°S and 55°N over oceans on 17 July 2015 are shown.

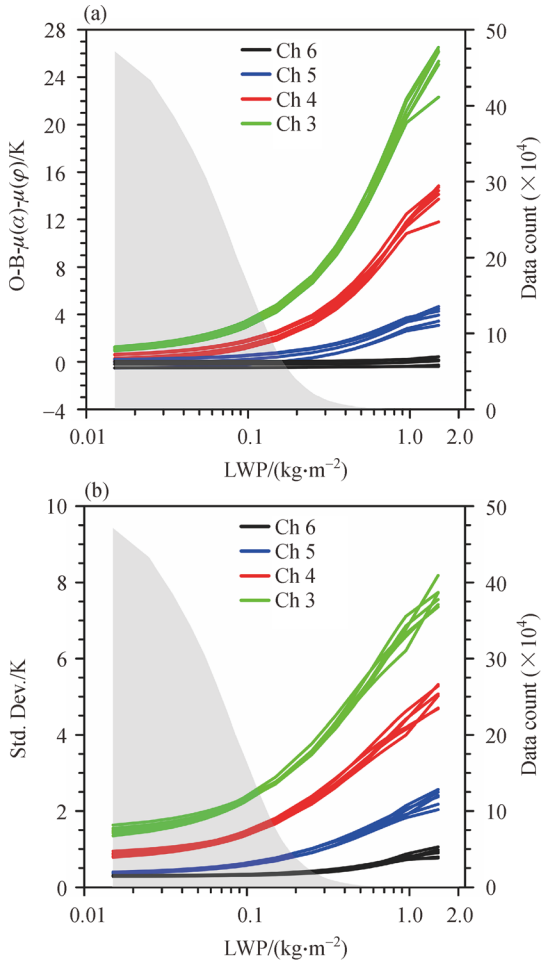

Fig. 12 Same as Fig. 11 but for data after the bias correction on 17 July of the years 2012–2017. The light gray shading shows the total data counts (right ordinate).

16–17 was used to exclude those points with IWP greater than or equal to 0.01 kg·m^{-2}. Each channel examined shows different degrees of increase in corrected bias as LWP increases. From channel 3 to channel 6, the sensitivity of corrected O-B to LWP in each channel decreases more and more as the detection height increases. The LWP has little effect on the mean biases of channel 6. In the absence of ice, the differences in clear-sky bias-corrected O-B-$\mu(\alpha)$-$\mu(\varphi)$ for ATMS channels 3–6 increase systematically as LWP increases. Lower-level, lower-frequency channels have larger positive biases. The impacts of LWP on channel 6 are negligible when LWP is less than 0.5 kg·m^{-2}. The biases under liquid cloudy conditions can be significantly reduced using the dependence of corrected O-B on LWP. Further investigation is required.

The characterization of ATMS biases is an important step for NWP applications and climate studies if ATMS data is to be linked to NOAA MSU/AMSU time series, i.e., a long-term fundamental climate data record for climate monitoring. This study further demonstrates the usefulness of the NWP 6-h forecast fields for characterizing the post-launch performance of microwave instruments. We plan to extend this work to the AMSU-A and the MHS onboard the NOAA-15, -18, and-19, and MetOp-A and-B satellites. This will require spatially collocated MHS and AMSU-A FOVs. Zou et al. (2017) have demonstrated that combining AMSU-A and MHS into a single data stream resulted in a more significant positive impact on quantitative precipitation forecasts than when AMSU-A and MHS radiance data were not collocated but rather, digested in data assimilation systems in two separate Binary Universal Form for the Representation of meteorological data files.

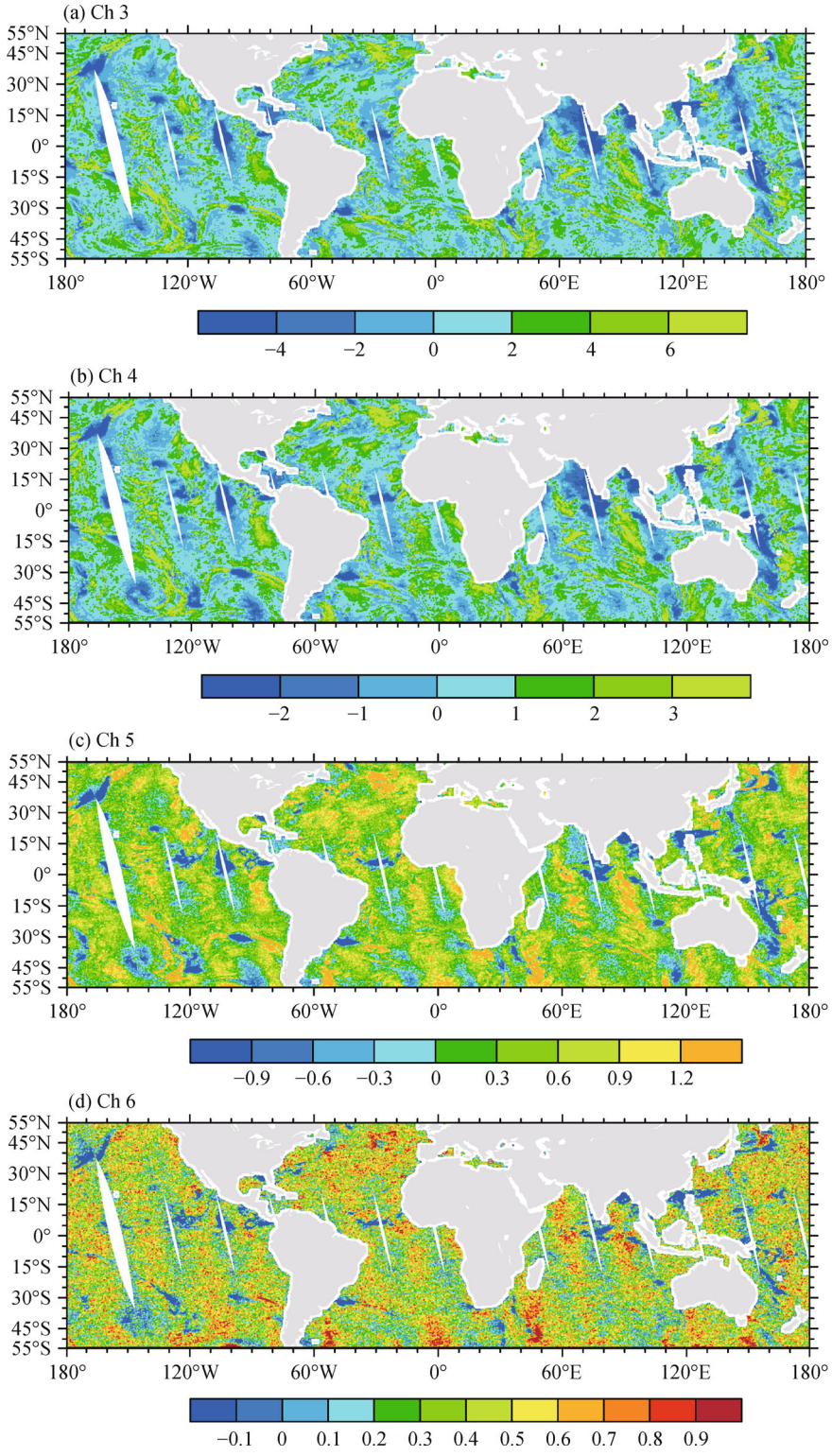

Fig. 13 Spatial distributions of the differences in brightness temperature (unit: K) between observations and CRTM model simulations without scan-, latitude-, and LWP-dependent biases for ATMS channels 3–6 (panels (a) to (d), respectively) from ascending nodes within 55°S and 55°N over oceans on 17 July 2015.

Acknowledgements The author was supported by the National Key R&D Program of China (No. 2018YFC1507302), and the Mathematical Theories and Methods of Data Assimilation supported by the National Natural Science Foundation of China (Grant No. 91730304).

References

Auligné T, McNally A P, Dee D P (2007). Adaptive bias correction for satellite data in a numerical weather prediction system. Q J R Meteorol Soc, 133(624): 631–642

Bormann N, Fouilloux A, Bell W (2013). Evaluation and assimilation of ATMS data in the ECMWF system. J Geophys Res Atmos, 118(23): 12970–129890

Dee D P (2005). Bias and data assimilation. Q J R Meteorol Soc, 131 (613): 3323–3343

Doherty A, Atkinson N, Bell W, Smith A (2015). An assessment of data from the advanced technology microwave sounder at the Met Office. Adv Meteorol, 2015: 956920

Han Y, Weng F, Liu Q, van Delst P (2007). A fast radiative transfer model for SSMIS upper atmosphere sounding channels. J Geophys Res Atmos, 112(D11): D11121

Karbou F, Gérard É, Rabier F (2006). Microwave land emissivity and skin temperature for AMSU-A and-B assimilation over land. Q J R Meteorol Soc, 132(620): 2333–2355

Karbou F, Gérard É, Rabier F (2010a). Global 4DVAR assimilation and forecast experiments using AMSU observations over land. Part I: impacts of various land surface emissivity parameterizations. Weather Forecast, 25(1): 5–19

Karbou F, Rabier F, Lafore J, Redelsperger J, Bock O (2010b). Global 4DVAR assimilation and forecast experiments using AMSU observations over land. Part II: impacts of assimilating surface-sensitive channels on the African monsoon during AMMA. Weather Forecast, 25(1): 20–36

Tian X, Zou X (2016). ATMS- and AMSU-A-derived hurricane warm core structures using a modified retrieval algorithm. J Geophys Res Atmos, 121(21): 12630–12646

Wang X, Zou X (2012). Quality assessments of Chinese FengYun-3B Microwave Temperature Sounder (MWTS) measurements. IEEE Transactions on Geoscience and Remote Sensing, 50(12): 4875–4884

Wang X, Zou X, Weng F, You R (2012). An assessment of the FY-3A microwave temperature sounder using the NCEP numerical weather prediction model. IEEE Transactions on Geoscience and Remote Sensing, 50(12): 4860–4874

Weng F (2007). Advances in radiative transfer modeling in support of satellite data assimilation. J Atmos Sci, 64(11): 3799–3807

Weng F, Zou X, Wang X, Yang S, Goldberg M D (2012). Introduction to Suomi national polar-orbiting partnership advanced technology microwave sounder for numerical weather prediction and tropical cyclone applications. J Geophys Res Atmos, 117: D19112

Xu X, Zou X (2018). A modified ice water path retrieval algorithm applicable to the ATMS. Tellus A: Dynamic Meteorology and Oceanography, 71: 1–14

Zhao L, Weng F (2002). Retrieval of ice cloud parameters using the Advanced Microwave Sounding Unit. J Appl Meteorol, 41(4): 384–395

Zou X, Lin L, Weng F (2014). Absolute calibration of ATMS upper level temperature sounding channels using GPS RO observations. IEEE Transactions on Geoscience and Remote Sensing, 52(2): 1397–1406

Zou X, Qin Z, Weng F (2017). Impacts from assimilation of one data stream of AMSU-A and MHS radiances on quantitative precipitation forecasts. Q J R Meteorol Soc, 143(703): 731–743

Zou X, Weng F, Zhang B, Lin L, Qin Z, Tallapragada V (2013). Impacts of assimilation of ATMS data in HWRF on track and intensity forecasts of 2012 four landfall hurricanes. J Geophys Res Atmos, 118 (20): 11558–11576

Zou X, Zhuge X, Weng F (2016). Characterization of bias of Advanced Himawari Imager infrared observations from NWP background simulations using CRTM and RTTOV. J Atmos Ocean Technol, 33 (12): 2553–2567

AUTHOR BIOGRAPHIES

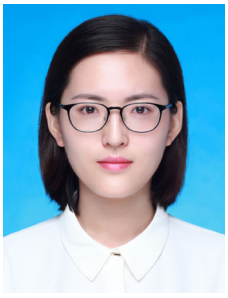

Qi Li received a B.S. degree in meteorology from Nanjing University of Information Science and Technology, Nanjing, China in 2016, where she is currently working toward a Master's degree in meteorology. Her research interests include satellite radiance data quality control and data assimilation.

Xiaolei Zou received her Ph.D degree from the Institute of Atmospheric Physics, Academia Sinica, Beijing, China in 1988.

She developed the National Meteorological Center (now the National Centers for Environmental Prediction) medium-range global forecast model 4D-Var system with full physics during 1989–1993, and the 5th generation Penn State/NCAR Mesoscale Model (MM5) 4D-Var system during 1993–1997. She has worked on GPS radio occultation data assimilation since 1993. From 1997–2014, she was a Professor in the Department of Earth, Ocean, and Atmospheric Science, Florida State University. Since Fall 2014, she has been working mainly on satellite data assimilation for quantitative precipitation forecasts and hurricane track and intensity forecasts at the Earth System Science Interdisciplinary Center, University of Maryland. She has published over 165 papers in peer-reviewed journals.

Dr. Zou was the recipient of the 2008 American Meteorological Society Fellow Award for her outstanding contributions to the applications of satellite data in numerical-weather-prediction models and to education in data assimilation.